A Feed-forward Featured Cascade PI Control Strategy for Tram Active Steering

Xiaotao Ren * **Tobias Brack** * **Tom Morris** *

* *Traila AG, Trockenloostrasse 101, 8105 Regensdorf, Switzerland (e-mail: xiaotao.ren@traila.ch)*

Abstract: Active steering is a technique that allows a railway vehicle to steer itself by adjusting the angle of a wheelset in order to avoid contact between flange and rail. This can improve wear, ride comfort, safety, and energy efficiency. This article analyzes the control requirements of a tram vehicle driving through small radius curves (20..129 m). An analysis of the angle that an actively steered axle has to maintain reveals that entering and leaving a curve represent a quadratic disturbance to the angle. To deal with this disturbance, a cascade PI controller is proposed. The controller consists of two loops: an inner loop that controls the wheel angle and an outer loop that controls the lateral deviation of the tram. The controller parameters are designed using a linearized model of the tram and are validated by simulations. The results show that the cascade PI controller can effectively reduce the quadratic disturbance and improve the lateral performance of the tram in curves.

Keywords: Controller structure, Disturbance rejection, High-order integral, Systems with time-delays

1. INTRODUCTION

Since railway vehicles are not equipped with a steering system, the wheel alignment to the track is achieved using conical wheels and the wheel flange. Since the contact between the wheel flange and the rail can create severe noise and wear of wheel and rail, numerous development and research projects tried to solve this issue by means of an actively steered systems, mostly related to existing standard-gauge railway bogies Hur et al. (2020, 2019); Mei and Goodall (2003); Mei et al. (2005).

However, said wheel flange contact and the related problems are of particular importance in tramway systems, where small curve radii and the less pronounced conical shape or independent wheels leads to frequent flange contact Wei (2014). Therefore, the Swiss company Traila AG is developing a novel active steering technology that allows a tram to steer itself through a curve by adjusting the angle of the wheels relative to the track Heinrich and Urbinati (2022); Morris et al. (2023); Heinrich and Urbinati (2023). This can improve ride comfort, safety, and energy efficiency of the tram, as well as reduce the wear and tear of the track and the wheels, thus minimizing emissions of fine dusts and maintenance costs for both vehicles and infrastructure.

For this purpose a single-axle wheelset with independent wheels has been developed that can actively rotate with respect to the tram wagon, using a hydraulic linear actuator. Using an onboard track-localization system, the relative position of the wheelset to the track is determined and fed into a controller that drives the actuator, thus forming a closed loop system that enables the active steering of the vehicle. This system has been successfully implemented in a discarded high-floor tram from Verkehrsbetriebe Zurich, Switzerland (VBZ Be 4/6 (Tram 2000)), where the rear bogie has been replaced by said hydraulically actuated single axle wheelset, cf. Fig. 1.

2. TRAM KINEMATICS

In order to effectively design the controller such that the flange contact is minimized, a thorough understanding of the kinematic behavior of a driving tram and the expected sensor reading is necessary.

As a representative of numerous tram designs, we particularly highlight the T2000 model, which consists of two wagons connected by a Jacobs bogie, cf. Fig. 2. As an initial approximation, we presume that the bogies self-center on the track through flange contact, while the rear is actively controlled without flange contact. The yaw angles of each wheelset are defined as the angle between the connection of the pivot points and the normal to the wheel axis. The connection length is defined by the wheelbase P of the vehicle.

2.1 Sensor Equation

The active rear axle is equipped with a sensor in front of the right wheel with a distance D from the center of the wheel. As shown in Fig. 3, the sensor measures the distance Y to the rail, given as

$$Y = \frac{M}{2}\left(1-\cos(\beta)\right) + D\sin(\beta) + \int V\sin(\beta)\mathrm{d}t\,, \qquad (1)$$

where M is the gauge width, V the tram speed and D the distance between wheel axle and sensor position. Assuming constant speed V and small angle of attack β, (1) can be linearized to

Fig. 1. Traila Test Tram with replaced rear bogie at the VBZ area in Zurich, Switzerland.

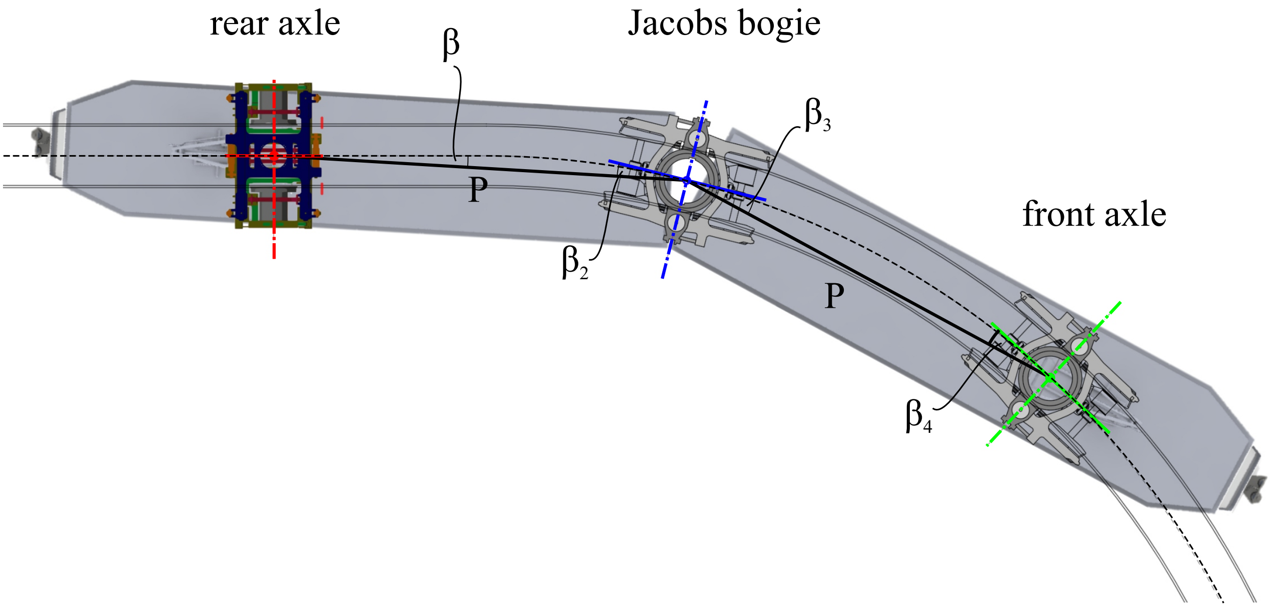

Fig. 2. T2000 test tram top view and angle definitions. The original pivoting bogies are used on the front wagon and Jacobs bogie, while the rear bogie has been replaced by a single-axle, actively pivoting wheelset.

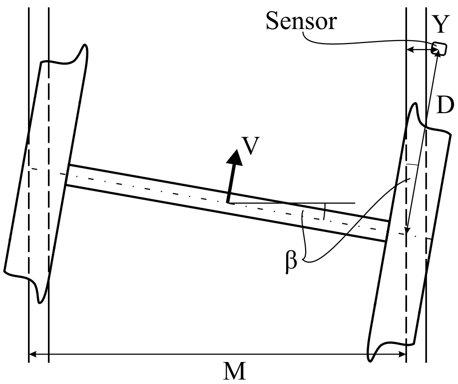

Fig. 3. Simplified drawing of the (active) rear wheelset on the track. The relative position Y between wheel and track is measured by a sensor attached to the wheelset at a distance D from the wheel axis.

$$Y = D\beta + V \int \beta \mathrm{d}t\,. \tag{2}$$

Considering the angle of attack β as an input to the axle, the driving motion of the tram measured by a sensor reading the relative position on the track can be regarded as a PI (proportional and integral) element.

2.2 *Tram driving through a curve*

To analyze the development of the ideal angle of attack, that is, the target of the control, a single wagon only with the actively controlled axle in the rear is considered. The Jacobs bogie is simplified by a single axle. The wagon is simplified to a fixed distance line connection between the two pivot points that follow a given trajectory. The trajectory is modelled as a circle segment of radius R and angle α connecting two straight line tracks, as depicted in Fig. 4. The entire track is laid out horizontally with no vertical gradient involved.

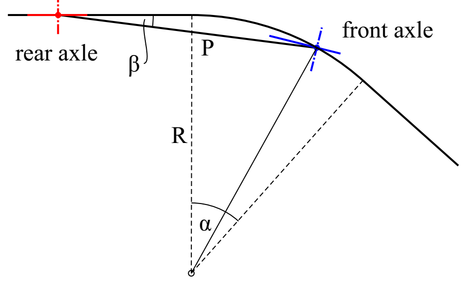

Fig. 4. Simplification of a railway vehicle with two wheelsets to two points with fixed distance moving on a given trajectory.

The driving through a curve can be divided into three distinct phases. The first phase is entering the curve where the front axle is already in the curve and the rear axle is still in the straight line. In this phase the target steering angle β is given by

$$\beta^{(1)} = \sin^{-1}\left(\frac{R(1-\cos\alpha)}{P}\right) . \tag{3}$$

Considering the front axle driving a constant tangent speed V, $\alpha = V/R \cdot t$, hence β can be approximated as

$$\beta^{(1)}(t) \approx \frac{V^2}{2PR}t^2 , \tag{4}$$

assuming $R > P$. The time t is zero when the front axle enters the curve. The second phase describes the situation where the full wagon is in the curve, hence

$$\beta^{(2)}(t) = \sin^{-1}\left(\frac{P}{2R}\right) \approx \frac{P}{2R} \tag{5}$$

The third phase is leaving the curve, with the front axle on the straight track and the rear axle still in the curve. Similarly to the scenario of entering the curve, the steering angle has the form

$$\beta^{(3)}(t) \approx \frac{P}{2R} - \frac{V^2}{2PR}t^2 , \tag{6}$$

where $t = 0$ when the front axle leaves the curve.
It is evident from (4)-(6) that the active steering controller must address a quadratic disturbance to effectively maintain the rear axle on its optimal trajectory when entering and leaving the curve. Additionally, it can be noted that for a tram with a fixed wheelbase P, this quadratic disturbance is directly proportional to the square of the speed and inversely proportional to the curve radius R.
To check that this theoretical description matches the reality, we used the T2000 test vehicle to acquire the angle data using angle encoders installed at every wheelset. Since we cannot use the rear axle directly due to the controller influence, we investigate the Jacobs bogie angle β_2, which is approximately equal to the rear axle angle target angle β. Figure 5 shows the comparison between (3), labeled "theory" and the measurement result for two different curve radii. The plot demonstrates excellent agreement, confirming the quadratic increase or decrease of the target angle during the phases.

The equations are formulated by modeling the wagon as a rigid body projected onto the ground. Vehicle dynamics are simplified into two interconnected bodies, while structural dynamics are disregarded. The nuanced variations depicted in Fig. 5 arise from comprehensive vehicle dynamics, structural deformations, imperfect tangential tracking of the bogie, and track deformations.

3. CONTROL SYSTEM DESIGN

The control diagram depicted in Fig. 6 shows the relevant elements of the active steering control loop.

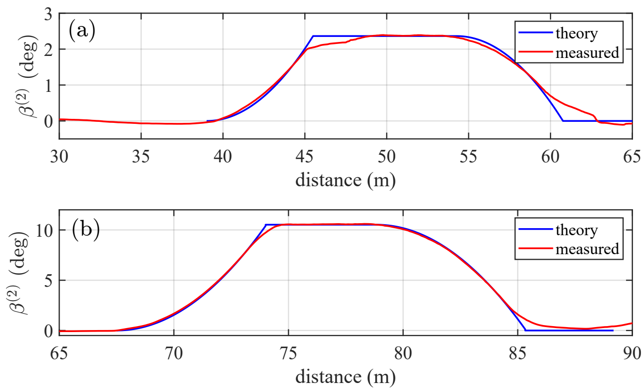

Fig. 5. Development of the rear Jacobs bogie angle $\beta_2 \approx \beta$ of the T2000 test tram while driving through a curve. Comparison between theory (4)-(6) and experiment. (a) $R = 79\,\text{m}$, $\alpha = 11\,\text{deg}$; (b) $R = 18\,\text{m}$, $\alpha = 37\,\text{deg}$.

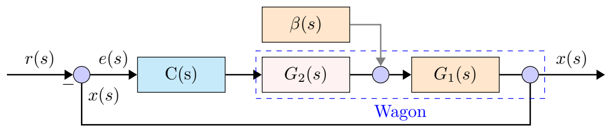

Fig. 6. Diagram of control system

The plant to be controlled, denoted as $G(s)$, represents the tram vehicle and is characterized by two transfer functions in series,

$$G(s) = \underbrace{\frac{Ds+V}{s}}_{G_1(s)} \cdot \underbrace{\frac{1}{L} \cdot \frac{1}{\tau s+1}}_{G_2(s)} , \tag{7}$$

where $G_1(s)$ describes the kinematics of the tram, cf. (2) and $G_2(s)$ is the transfer function of the actuation, which can be considered as a first-order delay system with gain $1/L$ (that is, the relation between actuator stroke and angle) and time constant τ. The actuator receives a stroke command from the controller $C(s)$ and changes the steering angle. The effect of the trajectory is introduced as an angle disturbance $\beta(s)$, where the disturbance transfer function for both entering and leaving a curve has the highest order of two in the time-space. In building the control model, only the entering phase is discussed. The designed control would be equally suitable for the leaving phase as well as the curving phase. Following from (4), the transfer function of the disturbance has the form

$$\beta(s) = \frac{V^2}{PR}\frac{1}{s^3} . \tag{8}$$

This third-order load disturbance, devoid of poles in both the left and right half s-planes, deviates from conventional systems. Consequently, designing an appropriate controller demands special attention, Wu et al. (2022).

The output of the control system, as shown in Fig. 6, is the sensor lateral position $x(s)$

$$x(s) = \frac{CG_2G_1}{1+CG_2G_1}r(s) + \frac{G_1}{1+CG_2G_1}\beta(s) , \tag{9}$$

where the set point is zero lateral position $r(s) = 0$. Therefore, the system error $e(s)$ has the form

$$e(s) = -\frac{G_1}{1 + CG_2G_1}\beta(s)\,. \tag{10}$$

Consider a well-designed control system ensuring strict stability and we employ the final value theorem. The expression for the steady-state error is

$$e_{\text{ss}} = \lim_{t\to\infty} e(t) = -\lim_{s\to 0} \frac{sG_1}{1 + CG_2G_1}\beta(s)\,. \tag{11}$$

The objective now is to design a controller $C(s)$ that ensures that the steady-state error is either zero or falls within an acceptable range even if the disturbance $\beta(t)$ is of quadratic shape. Assuming a controller transfer function

$$C(s) = K_p + \frac{K_i}{s} + \frac{K_{ii}}{s^2} + \frac{K_{iii}}{s^3}\,, \tag{12}$$

where $K_p, K_i, K_{ii}, K_{iii}$ are gains to be determined. By combining (12) with (11), the system steady error becomes

$$e_{\text{ss}} = \lim_{s\to 0} \frac{-K_0(Ds + V)s}{Ls^4 + (Ds + V)(K_p s^3 + K_i s^2 + K_{ii} s + K_{iii})}\,, \tag{13}$$

where $K_0 = V^2L/(PR)$ is the plant parameter independent of the controlling gains. Equation (13) illustrates that employing a classic PI controller, where $K_{ii} = K_{iii} = 0$, results in an infinite steady-state error. Consequently, the system error exhibits an approximate linear growth over time. Conversely, adopting a controller featuring a second-order integral, with $K_{ii} > 0$ and $K_{iii} = 0$, yields a constant steady-state error. Finally, utilizing a third-order integral configuration will achieve a system with zero steady-state error. Hence

$$e_{\text{ss}} = \begin{cases} 0, & \text{if } K_{iii} > 0 \\ -K_0/K_{ii}, & \text{if } K_{ii} > 0, K_{iii} = 0 \\ \infty, & \text{if } K_{ii} = K_{iii} = 0\,. \end{cases} \tag{14}$$

However, implementing a controller with a third-order integral presents complications. Multiple loops become necessary, and tuning the control parameters within each loop poses a significant challenge. Opting for a controller featuring a second-order integral offers a favorable compromise. During tram operation, minor lateral discrepancies can be accommodated. Adjusting the controlling parameter K_{ii} adapts the steady-state error value.

3.1 Cascade PI

A polynomial with a double integrator can be factorized into two first-order integrators,

$$C(s) = (K_{p1} + \frac{K_{i1}}{s})(K_{p2} + \frac{K_{i2}}{s}) = C_1(s)\cdot C_2(s) \tag{15}$$

where $K_{p1}, K_{i1}, K_{p2}, K_{i2}$ are the controlling gains to be determined. In applications, a derivative term $K_d s$ can be added to $C_1(s)$, $C_2(s)$ or both.

The block diagram depicted in Fig. 7 illustrates the implementation of cascade proportional-integral (PI) control. Cascade PI control is extensively utilized across various industries, with a typical application being the position control of a motor, for instance, Gürocak (2015). Additionally, there are readily available methods for tuning the control parameters within cascade PI systems. To ensure

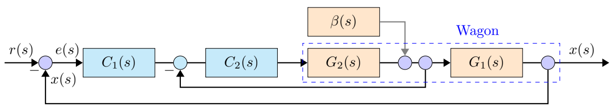

Fig. 7. Block diagram of cascade PI

minimal interference of the inner loop on the outer loop, the response of the inner loop must be faster than that of the outer loop.

3.2 Feed-forward Control

Understanding the characteristics of quadratic disturbances allows for a feed-forward control strategy, Guzmán and Hägglund (2021). This approach involves anticipating the disturbance and feeding it forward to $G_2(s)$ to mitigate its impact on $G_1(s)$. As shown in Fig. 8 in the signal

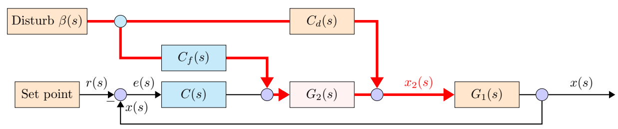

Fig. 8. Block diagram of feed-forward control as indicated in the thickened red line.

path in red color, design a feed-forward control G_f to eliminate the disturbance. Consider only the effect of the disturbance. The transfer function writes,

$$\frac{x_2(s)}{\beta(s)} = G_fG_2 + G_d = 0 \Longrightarrow G_f = -\frac{G_d}{G_2} \tag{16}$$

where G_d relies on how the disturbance is measured. Let $G_d(s) = 1$ and given $G_2(s)$ as in (7), we have the feed-forward transfer function,

$$G_f = -L\frac{\tau s + 1}{\tau_f s + 1} \Longrightarrow \frac{x_2(s)}{\beta(s)} = \frac{\tau_f s}{\tau_f s + 1} \tag{17}$$

τ_f is added to the denominator to make the system proper. Hence, despite possessing precise knowledge of the dynamics of the disturbance to be managed, designing a feed-forward control system to entirely eliminate this disturbance before it affects G_1 within the system remains practically unattainable. Relying solely on feed-forward control may increase the errors due to the absence of corrective measures. On the other hand, it can be observed from (17) that incorporating the feed-forward decreases the disturbance by one order before transmitting the signal to G_1.

Therefore, integrating a feedback term is essential to ensure that the tracking error approaches zero or converges to an acceptable value. A system as in Fig. 8 with feed-forward and a controller as in (12) has the output,

$$x(s) = \frac{CG_2G_1}{1 + CG_2G_1}r(s) + \frac{G_1\frac{\tau_f}{\tau_f s+1}s}{1 + CG_2G_1}\beta(s) \tag{18}$$

Calculate the system steady-state error by considering zero set point,

$$e_{ss} = \begin{cases} 0, & \text{if } K_{ii} > 0 \\ -\tau_f K_0/K_i, & \text{if } K_i > 0, K_{ii} = 0 \end{cases} \tag{19}$$

A combination of feed-forward with a classical PI controller may result in a constant steady-state error. Conversely, employing a feed-forward enhanced cascade PI controller, as in Fig. 9, has the potential to achieve zero steady-state error in the presence of quadratic disturbances.

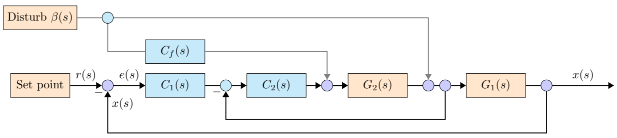

Fig. 9. Diagram of feed-forward featured cascade PI controller

4. EXPERIMENT

Three controller arrangements were tested: the first one is the cascade PI, denoted as PII, depicted in Fig. 7; the second involves feed-forward with a classical PI, abbreviated as F-PI; and the third utilizes feed-forward with a cascade PI configuration, abbreviated as F-PII, as shown in Fig. 9. The tram's geometry includes a wheelbase of $P = 6.5$ m, a distance of $D = 0.36$ m between the wheel's vertical axis and the sensor, and a lever length of $L = 0.78$ m for hydraulic actuation. Various tram rolling speeds were applied, such as $\{6, 12, 18\}$ kmh, along with different radii of curvature, ranging from $\{20, 50, 129\}$ m. As for the requirements for the test Tram, the lateral allowance is 8 mm and the designed lateral target is set to 5.5 mm.

In a cascade PI configuration, the bandwidth of the inner loop is typically 5 to 10 times higher than that of the outer loop. As an illustration, consider a tram traveling at 6 kmh negotiating a curve with the following control gains:

$$C_2(s) = 0.5 + \frac{7}{s}, \qquad C_1(s) = 0.38 + \frac{1}{6.3s} \tag{20}$$

the closed-loop bandwidths for the inner and outer loops are 7.36 rad/s and 0.98 rad/s, respectively. The control errors for these three arrangements are plotted in Fig. 10. In this experiment, the feed-forward time constant $\tau_f = 3$ sec.

Three controllers satisfy the requirement of an 8 mm lateral limit for the current speed and curve radius configuration. However, as the curve sharpens and the rolling speed increases, the disturbance becomes more severe. Since the dead time in the system is neglected and the reference point is zero, The control error is approximately proportional to the square of the velocity V^2 and inversely proportional to the curve radius for the same control gains.

The upper sub-figures in Fig. 10 and Fig. 11illustrate the errors under the assumption of an infinite quadratic disturbance. This is intended to demonstrate the convergence characteristics of steady errors, as derived in equations (14) and (19). Meanwhile, the lower sub-figure

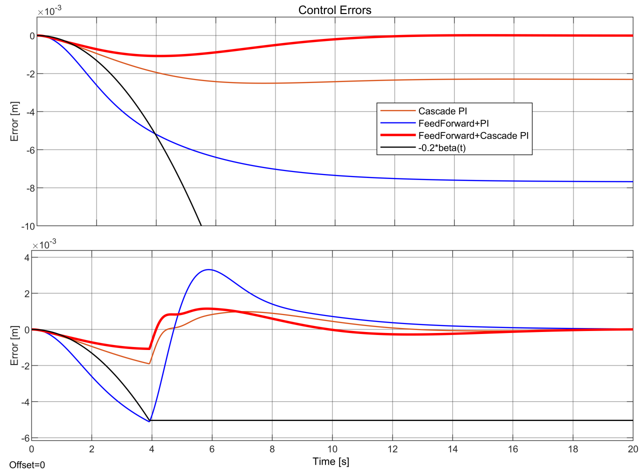

Fig. 10. Control errors of three control arrangements. The curve radius is $R = 129$ m and the rolling speed is $V = 6$ kmh. The F-PI has a $C(s) = 1 + 1/s$. The disturbance is scaled by -1/5 for plotting purposes.

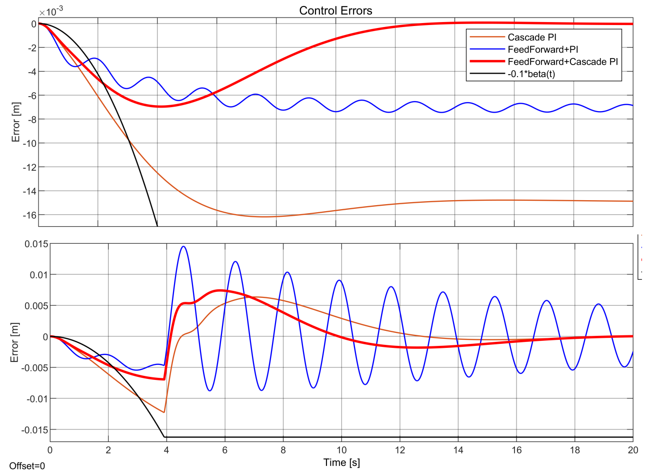

Fig. 11. Control errors of three control arrangements. The curve radius is $R = 20$ m and the rolling speed is $V = 6$ kmh. The F-PI has a $C(s) = 0.5 + 7/s$. The disturbance is scaled by -1/10 for plotting purposes.

depicts the control error considering both the quadratic disturbance and transition into a constant value. In this paper, the stage of leaving the curve is experimented. Both the PII and F-PI exhibit constant error, whereas F-PII achieves zero control error. The advantages of employing feed-forward mechanisms are apparent, notably in significantly reducing response times. For addressing extended quadratic disturbances, F-PI appears adequate. Nonetheless, it requires a high integral gain to converge rapidly, resulting in system oscillation. In comparison, cascade PI control can manage such disturbances with acceptable overshoot. However, as depicted in Fig. 11, control error escalates linearly. Moreover, with increasing tram rolling speed, overshooting can be severe enough to cause flange contact.

5. CONCLUSION

Maintaining the optimal angle of an actively steered wheelset of a railway vehicle with two wheelsets on one wagon requires a controller that can deal with quadratic disturbances. These disturbances manifest prominently during critical phases when the vehicle maneuvers into or out of a curve. This article presents a feed-forward enhanced cascade PI controller (F-PII) to deal with quadratic load disturbance. Through rigorous analysis and extensive experimental validation, we scrutinize the nature and impact of these disturbances. The performance of the F-PII is compared with feed-forward with a classical PI and a cascade PI with no feed-forward. Experimental Results indicate that the combined implementation of feed-forward and cascade PI is essential for effectively neutralizing load disturbances. This combination effectively eliminates the load disturbance swiftly.

REFERENCES

Guzmán, J.L. and Hägglund, T. (2021). Tuning rules for feedforward control from measurable disturbances combined with pid control: a review. *International Journal of Control*, 97(1), 2–15. doi: 10.1080/00207179.2021.1978537.

Gürocak, H. (2015). *Industrial Motion Control: Motor Selection, Drives, Controller Tuning, Applications*. Wiley. doi:10.1002/9781118403211.

Heinrich, S. and Urbinati, S. (2022). Investigation of passive steering concepts using matlab simulink for their application in a modified tram 2000. *Getriebetagung 2022*, 181–182. doi:10.30819/5552.15.

Heinrich, S. and Urbinati, S. (2023). Fast analytical wheel-rail contact modelling for realtime capable mbs in hil using matlab simulink. In *Proceedings of the 28th Symposium of the International Association of Vehicle System Dynamics, IAVSD 2023*.

Hur, H., Shin, Y., and Ahn, D. (2020). Analysis on steering performance of active steering bogie according to steering angle control on curved section. *Applied Sciences*, 10(12). doi:10.3390/app10124407.

Hur, H., Shin, Y., Ahn, D., and Ham, Y. (2019). Steering performance evaluation of active steering bogie to reduce wheel wear on test line. *International Journal of Precision Engineering and Manufacturing*, 20(9), 1591–1600. doi:10.1007/s12541-019-00167-0.

Mei, T. and Goodall, R. (2003). Recent development in active steering of railway vehicles. *Vehicle System Dynamics*, 39(6), 415–436. doi:10.1076/vesd.39.6.415.14594.

Mei, T., Shen, S., Goodall, R., and Pearson, J. (2005). Active steering control for railway bogies based on displacement measurments. *IFAC Proceedings Volumes*, 38(1), 586–591. doi:10.3182/20050703-6-CZ-1902.00498. 16th IFAC World Congress.

Morris, T., Heinrich, S., Ronci, A., and Cervello, S. (2023). Development and testing of a new active steering system for light rail transportation. *20th Int. Wheelset Congress Chicago*.

Wei, Y. (2014). *Spurführungsregelung eines aktiv gelenkten Radpaars für Straßenbahnen*. KIT Scientific Publishing, Karlsruhe. doi:10.5445/KSP/1000041687.

Wu, Z., Shi, G., Li, D., Liu, Y., and Chen, Y. (2022). Active disturbance rejection control design for high-order integral systems. *ISA Transactions*, 125, 560–570. doi:10.1016/j.isatra.2021.06.038.